# Evaluation of Detrainment and Microphysics Parameterization in the NCEP GFS Single-Column Model

*Y. Luo*
*National Institute of Aerospace*
*Hampton, Virginia*

*S. K. Krueger*
*University of Utah*
*Salt Lake City, Utah*

## Introduction

Representation of clouds in current General Circulation Models (GCMs) needs evaluation and improvement for climate prediction (e.g., Cess et al. 1996). Cloud Resolving Models (CRM) and Single Column Models (SCMs) along with new valuable observational datasets are useful tools for this objective (Randall et al. 1996, Randall 2003). Large-scale forcing data produced by the Atmospheric Radiation Measurement (ARM; Stokes and Schwartz 1994, Ackerman and Stokes 2003) program at the Southern Great Plains site for the summer 1997 Intensive Operation Period (IOP) were used to drive a CRM and a SCM. Simulations from these two models were used to evaluate the model cirrus properties and physical processes through a comparison with the km-scale observations obtained from the ARM program. The CRM was found to reproduce most features as revealed by the observations (Luo et al. 2003), and subsequently both the km-scale observations and the CRM results were used to evaluate the SCM. The objectives of our study are therefore to show the results of our evaluation, to demonstrate a new evaluation method, and to encourage greater use of cloud-scale observations on their native scale. We present our study in a three-part series of papers.

In the Part I (Luo et al. 2004), the SCM km-scale cirrus properties were analyzed and compared to the cirrus observations and retrievals from the cloud radar by applying the SCM's assumptions of cloud overlap and cloud horizontal inhomogeneity to its profiles of cloud fraction and cloud water/ice mixing ratio. The SCM cirrus cloud-base height and physical thickness depend on the assumption of cloud overlap and, more significantly, on whether snow is considered as cloud. Regardless of the overlap assumption used and no matter if snow is included or not, the SCM thin cirrus (as defined by Mace et al. 2001) Ice Water Path (IWP) distribution and Ice Water Content (IWC) distribution are skewed to large values and IWCs decrease with cloud physical depth instead of increasing as observed. When snow is not included in the SCM, too many SCM cirrus clouds occur at a single model level.

Here we present Part II of our study. We expect that the cirrus properties in a model are closely related to the cumulus detrainment and cloud ice microphysical processes in the model. Since no observational data of detrainmental and microphysical rates were available to evaluate the SCM's representation of detrainment and cloud ice sublimation, we analyzed and compared the results from simulations by the SCM and the CRM, where each simulation was driven by the large-scale forcing data from the

variational analysis (Zhang and Carr 1997, Zhang et al. 2001) for the ARM SGP site summer 1997 IOP. Detailed descriptions of the CRM and SCM simulations are provided by Luo et al. (2003) and (2004), respectively. To evaluate other cloud ice microphysical processes in the SCM, we developed a 1-D cirrus model implemented with both the SCM and the CRM's microphysical schemes. The evolution of ice clouds in a saturated layer is studied using this 1-D cirrus model. The evaluation of the SCM's detrainment parameterization is presented in Section 2, and the evaluation of the SCM's microphysical schemes is presented in Section 3. We summarize and discuss our results in Section 4.

In Part III (Krueger and Luo) and Luo and Krueger (2004), we will compare the occurrence frequencies and radiative forcing of various cloud types in the SCM and the CRM with the estimates from pixel-level satellite observations.

## Evaluation of Cumulus Detrainment Parameterization

Detrainment of cloud condensate (liquid water or ice) is included in the SCM and many current large-scale models (e.g., Del Genio and Yao 1990, Ose 1993, Tiedtke 1993, Fowler et al. 1996) as a source for grid-mean stratiform cloud mixing ratio ( $q_i$ ). Detrainment occurs at convective cloud tops in the SCM, and deep convection is parameterized using a simplified Arakawa-Schubert scheme (1974) with only one cloud type considered (Pan and Wu 1995). The cloud top is randomly determined in the model as a level between the highest possible cloud top (neutral buoyancy level) and the level where the environment moist static energy is a minimum.

Including the effect of detrainment in $q_i$ prediction establishes a coupling between convective dynamics and stratiform anvil clouds formed at the tops of cumulus towers. However, evaluation of the detrainment parameterization is not straightforward. In reality cloud condensate is detrained from the active convective regions (convective cores) to the relatively inactive convective regions, as well as from the inactive convective region to the nonconvective (stratiform) region. The parameterized detrainment rate in a SCM depends on *which part is parameterized*: whether from active convective cores or from relatively inactive convective regions. In a CRM the calculated detrainment rate in a CRM depends on the partition between convective and stratiform regions as well (e.g., Tao et al. 1993). To obtain the detrainment rate of cloud condensate in the CRM, two methods were used to find the convective regions. One method is based on observations of the kinematic structures of meso-scale convective systems (Xu 1995). Using this method, convective regions consist of a convective "core" and two adjacent grid columns, where a core consists of at least one convective grid column. The horizontal distribution of the maximum cloud draft strength below the melting level ($w_{max}$) in a CRM grid column is used as the primary variable to find convective columns.

A grid column is convective if it satisfies one of the following conditions: (a) $|w_{max}|$ is at least twice as large as the average over the four adjacent grid columns, (b) $|w_{max}|$ is greater than 3 m $s^{-1}$, or (c) surface precipitation rate exceeds 25 mm $h^{-1}$. Results using this method are called $CRM_{xu}$ and should represent the detrainment from the inactive convective region to the stratiform region. The other method determines whether each grid point, instead of grid column as in the first method, is part of a convective core. A grid point is part of a convective core if it satisfies two conditions: (a) cloud liquid and ice water mixing ratio is greater than 1% of the saturation water vapor mixing ratio, and (b) vertical velocity is

larger than 1 $ms^{-1}$. Results analyzed using this method are called $CRM_{core}$ and should represent the detrainment from the convective cores to the inactive convective region.

The detrainment of cloud condensate in the CRM is due to the combined effects of airflow out of the convective region and changes in the area of the convective region. The profiles of detrainment of cloud ice (including large ice crystals or "snow") in the CRM and detrainment of cloud ice only in the SCM, averaged over the entire simulation period (29 days; summer 1997 IOP), are shown in Figure 1. The SCM values (solid line, Figure 1) are located between $CRM_{xu}$ (dotted line) and $CRM_{core}$ (dotted-dashed line) at almost all heights where detrainment occurs. The CRM's profiles have their largest values at around 9-10 km (250 to 300 mb), which is about 1 km above that of the SCM. The SCM time-averaged detrainment rate is between those from the CRM. The time-height distributions of the hourly cloud ice detrainment rate in the CRM and the SCM are illustrated by Figure 2. In the CRM both cloud ice and snow are detrained while only cloud ice is detrained in the SCM. Only the subperiod B is shown for illustration. However the same features are found for other periods of the IOP. ***Note that the values represent averages over the CRM domain and the SCM grid means respectively, i.e. the detrainment by cumulus cloud ensembles. In reality cumulus clouds at different stages of evolution coexist in the area at a certain time, and these clouds have various sizes and top-heights. Detrainment occurs at the tops of ensemble cumulus clouds (not a single one).*** The detrainment profiles in the two models differ significantly. Cloud condensate is detrained at one single level at a time in the SCM and detrainment occurs too sporadically with larger rates. Both $CRM_{xu}$ and $CRM_{core}$ show that in the CRM detrainment occurs over thicker layers and lasts for longer periods. As a result the distributions appear smoother in both time and height compared to detrainment distributions of the SCM.

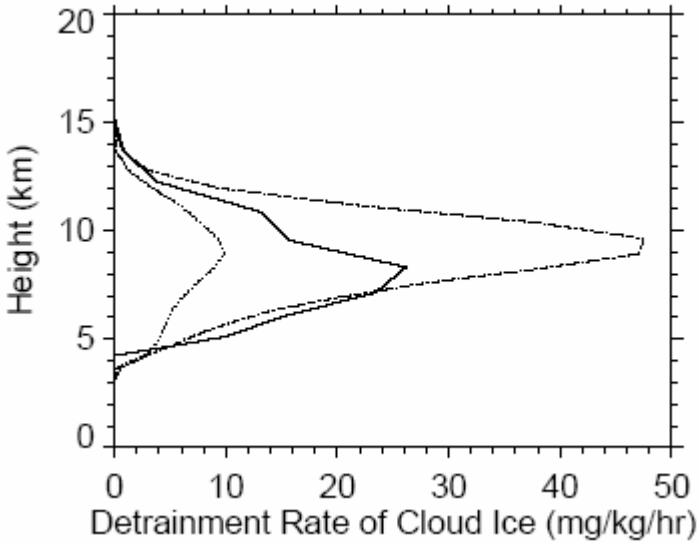


**Figure 1**. Profiles of detrainment of cloud ice (including large ice crystals or "snow") in the CRM and detrainment of cloud ice only in the SCM, averaged over the 29-day simulation period. See text for details.

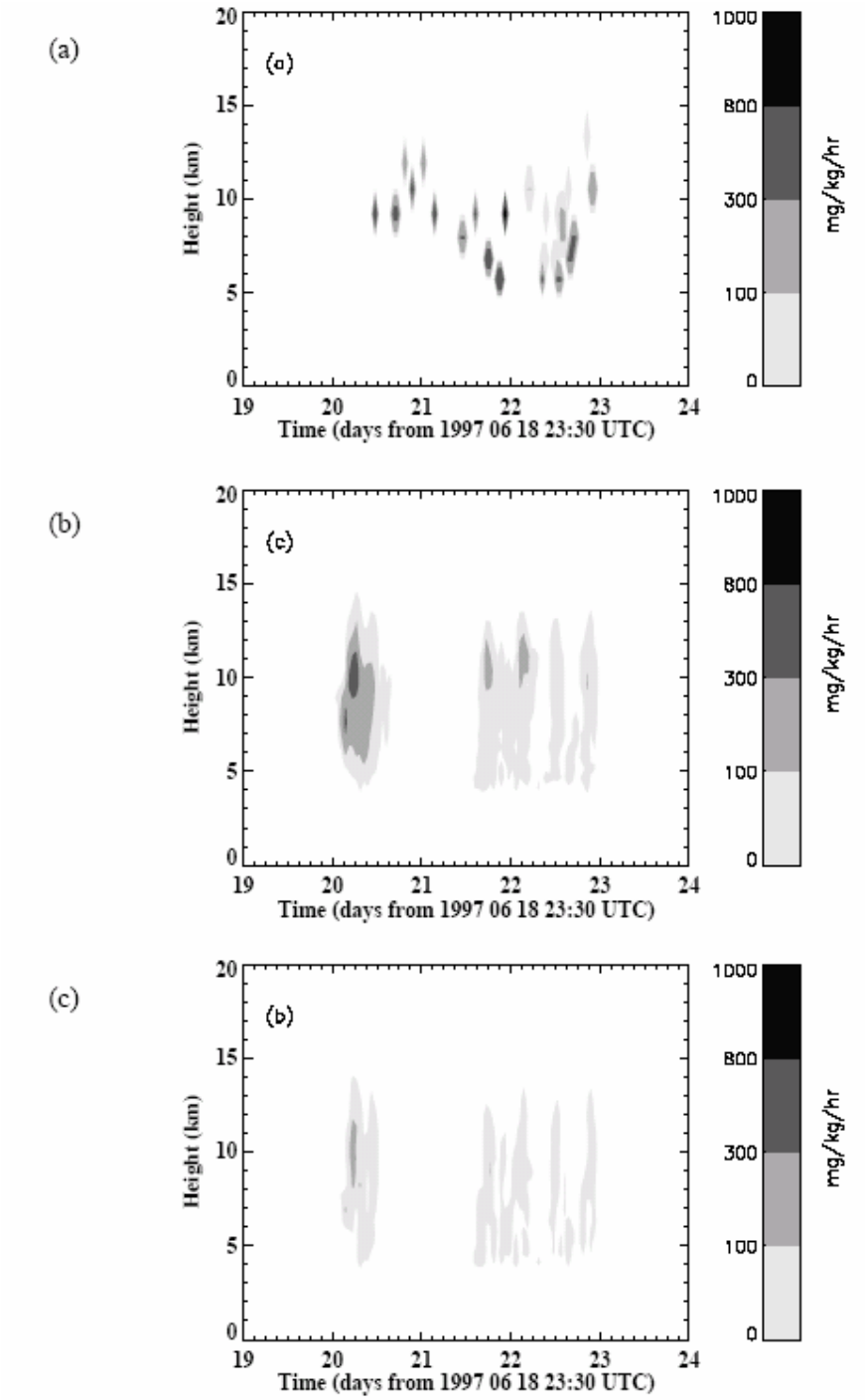


**Figure 2**. The time-height distributions of the hourly cloud ice detrainment rate in the SCM and CRM during a 5day subperiod of the IOP, starting at 23:30 UTC July 07 1997. (a) SCM. (b) $CRM_{core}$. (c) $CRM_{xu}$.

The fact that the SCM detrains in too thin layers can partly explain our findings that its thin cirrus IWC and IWP distributions skew toward large values and that too many thin cirrus layers occur at a single model level. If detrainment occurred in thicker layers, the cloud would be thicker for the same IWP.

This would decrease the IWC values for the detrainment-formed clouds and tend to correct these errors. If detrainment lasted for longer periods with the same total IWP, clouds would have smaller IWP and IWC. This would also tend to correct the errors.

The large-scale condensation/evaporation of cloud condensate and the interaction with precipitable hydrometeors (i.e., microphysical processes) determine the evolution of cloud water/ ice in a SCM grid, as do cumulus detrainment, large-scale advection, and diffusion. Due to lack of observations, large-scale horizontal advection of cloud condensate is not included in the SCM simulation. Vertical advection is also not included in the SCM simulation, where it is assumed that the upward transport by large-scale motion is balanced by gravitational drag.

We evaluate the SCM's microphysical schemes through a detailed comparison with the CRM results.

# Evaluation of Cloud Microphysics

## Description of the Simulations

We developed a 1-D cirrus cloud model and using this model performed a series of idealized simulations. Results from two of the idealized simulations are represented here. The two simulations start from the same initial profiles of temperature and moisture. The same amount of cloud ice (500 mg $kg^{-1}$) is put into a single saturated layer (360 to 380 mb) to represent the detrained cloud ice. Both simulations have a model top at 300 mb, a model bottom at 840 mb, a vertical interval of 20 mb, 27 vertical layers, and a 4-hour simulation period. Large-scale vertical velocity is zero in the two simulations. The microphysics for cloud ice and precipitation (snow) are represented differently in the two simulations. In one simulation, the same ice/snow microphysics as those used in the CRM (Lin et al. 1983, Lord et al. 1984, Krueger et al. 1995) are implemented. The forward scheme for the microphysical rates and the Adams-Bashforth scheme for the sedimentation rates are used. We call this simulation "Dcrm". The Dcrm simulation predicts snow mixing ratio and snow fall speed explicitly. The source terms of snow include the aggregation of ice crystals (SAUT), accretion of ice crystals by snow (SACI), and transformation of cloud ice to snow via the growth of Bergeron-process embryos (SFI), while the sink of snow is sublimation (SSUB). The snow flux at a level in the Dcrm simulation is diagnosed using

$$F_s = \rho q_s V_s \tag{1}$$

where $F_s$ is snow flux, ρ is air density, $q_s$ is snow mixing ratio, and $V_s$ is snow fall speed. In the other simulation, the same microphysics of cloud ice/snow as those in the NCEP SCM (Zhao and Carr 1997) were used. We call this simulation "Dscm". The Dscm simulation does not predict snow mixing ratio. It diagnoses snow flux $F_s$ at the bottom of each model layer using the same method as the NCEP SCM model; i.e. $F_s$ is the vertical integral of the net snow production by microphysics at/above that layer. This implicitly assumes that there is a balance between the net production of snow by microphysical processes and the falling out of snow within one time step. The cloud ice/snow microphysical processes included in Dscm simulation are aggregation of ice crystals (SAUT), accretion of ice crystals by snow (SACI), and sublimation of snow (SSUB). We diagnose the Dscm's $q_s$ from its $F_s$ by relating the $V_s$ to

$q_s$ using the same formula for $V_s$as that in the CRM. The time step interval was 20 seconds and 1800 seconds, and the total number of time steps was 720 and 8, for Dcrm and Dscm, respectively.

## Results from the Idealized Simulations

Figure 3 shows the profiles of $F_s$ and $q_s$ at 0.5, 1.0, 2.0, and 3.0 hr in Dcrm and Dscm simulations. It is obvious that the $F_s$ in the Dscm simulation extends to much lower layers compared to that in the Dcrm. Consequently the Dscm's $q_s$ which is diagnosed from its $F_s$, also extends too low compared to that explicitly predicted by the Dcrm. This demonstrates that the SCM diagnosed snow flux extends too low so that the cirrus layers are too thick and have too low base-heights when snow is included as part of cirrus. Neglecting diffusion and advection of snow, the prognostic equation for snow mixing ratio can be expressed by

$$\frac{\partial}{\partial t}q_s = S_{micro} - \frac{1}{\rho}\frac{\partial}{\partial z}\rho\overline{q_s V_s} \tag{2}$$

where $S_{micro}$ is net production of snow by microphysical processes. The SCM assumes a balance between the net production of snow and snow falling out within one time step. This assumption indicates that Eq. (2) is approximated by

$$\frac{\partial}{\partial t}q_s = 0 \tag{3}$$

an approximation that is not satisfied unless

$$V_s \gg \frac{\Delta z}{\Delta t}, \tag{4}$$

where $\Delta z$ is the vertical interval (about 1 km) of the SCM grid and $\Delta t$ is the time step interval for the SCM simulation (about 1000 s). Snow (large ice crystals) fall speeds seldom exceed1ms$^{-1}$ as suggested by observations (Heymsfield and Iaquinta, 2000) and the CRM simulations. Therefore, Eq. (3) is not satisfied and the balance assumption is not appropriate for snow in the SCM (and a global model) simulation. It should be more appropriate for rain because of a larger fall speed of rain (about 10 ms$^{-1}$).

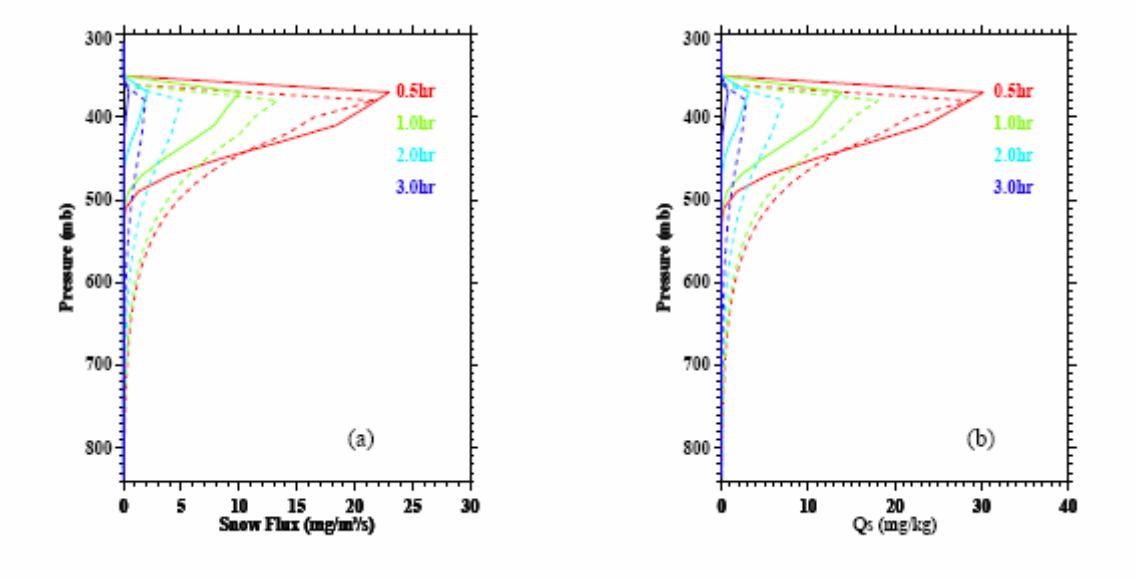


**Figure 3**. The profiles of snow flux (a) and snow mixing ratio (b) at 0.5, 1.0, 2.0, and 3.0 hr in Dcrm (solid lines) and Dscm (dashed lines) simulations.

In the Dscm simulation, the amount of $q_i$ at the layer where detrainment occurred decreases from 500 to 308 (0.5 hr), 191 (1.0 hr), 74 (2.0 hr) and 30 (3.0 hr) mg $kg^{-1}$, while that in the Dcrm simulation decreases to 220, 99, 21, and 5 mg $kg^{-1}$. The averaged time rate of change of qi by microphysical processes from 0.0 to 0.5 hr, 0.5 to 1.0 hr, and 1.0 to 2.0 hr are provided in Table 1. It seems that the decrease-rates of the detrained cloud ice (in the overcast situation) by all microphysical processes are comparable in the two simulations. The IWP and snow water path (SWP) are measurements of the total amounts of ice and snow, respectively, in an atmospheric column. Their values and those of IWP + SWP in the two simulations at 0.5, 1.0, 2.0, and 3.0 hr are listed in Table 2. We do not see significant differences in the change with time of IWP and SWP in the two simulations. However, the Dscm has more SWP than the Dcrm after half hour because of snow extending into a much thicker layer (Figure 3), and it has more IWP at all times.

**Table 1**. The averaged time rate of change of cloud ice mixing ratio (mg $kg^{-1}$ $s^{-1}$).

| | **0.0-0.5hr** | **0.5-1.0hr** | **1.0-2.0hr** |
|---|---|---|---|
| Dscm | 0.107 | 0.066 | 0.033 |
| Dcrm | 0.156 | 0.067 | 0.022 |

**Table 2**. Comparison of the IWP, SWP, and IWP+SWP (g $m^{-2}$) at 0.5, 1.0, 2.0, and 3.0 hr in the Dcrm and Dscm simulations.

| | time (hr) | 0.5 | 1.0 | 2.0 | 3.0 |
|---|---|---|---|---|---|
| SWP | Dcrm | 24 | 10 | 2 | 0.5 |
| | Dscm | 17 | 12 | 5 | 2 |
| IWP | Dcrm | 45 | 20 | 4 | 1 |
| | Dscm | 63 | 38 | 15 | 6 |
| SWP + IWP | Dcrm | 69 | 30 | 6 | 2 |
| | Dscm | 80 | 50 | 20 | 8 |

We examine the evolution of cloud ice and snow by each of the microphysical processes in the simulations. Figure 4a,b shows the profiles of the time-averaged rates (from 0 to 0.5 hr and 0.5 to 1.0 hr, respectively) of snow generation while Figure 4c provides those of the snow sublimation rates. The microphysical processes that may cause snow generation/increasing are SAUT, SACI and SFI in the Dcrm, and SAUT and SACI in the Dscm. In the Dcrm simulation the rate of aggregation of ice crystals (SAUT) was zero at all levels because the threshold amount of cloud ice to activate SAUT was 600 mg $kg^{-1}$, larger than the specified amount of detrained cloud ice (500 mg $kg^{-1}$). The generation of snow in the Dcrm simulation was originally through the Bergeron process (SFI), and then snow increased through both SFI and SACI. The SFI is the dominant term for snow production compared to SACI in Dcrm simulation. The mechanism of snow production in the Dscm simulation was only SAUT. The rate of SACI in the Dscm was calculated using

$$SACI = \exp(0.025 \times T_c) \times F_s \times q_i \tag{5}$$

where $T_c$ is temperature in degrees C, $F_s$ is the snow flux from above. In the simulation, $q_i$ was $c$ greater than zero only at the single layer where detrainment occurred. However, $F_s$ was zero for this layer and the layers above (Figure 3) so that SACI was zero at all layers. We conclude that the mechanisms of snow generation/ice decreasing in the two simulations are obviously different, though the net effects of microphysical processes on snow production are comparable. The magnitudes of snow sublimation rates are similar in the two simulations (Figure 5c). However, the snow flux extends too low in the Dscm simulation due to the balance assumption used (Eq. 3.2), and results in an overestimation of downward transport of water vapor through snow sublimation. This is also demonstrated by the change of relative humidity (Figure 5) in the two simulations.

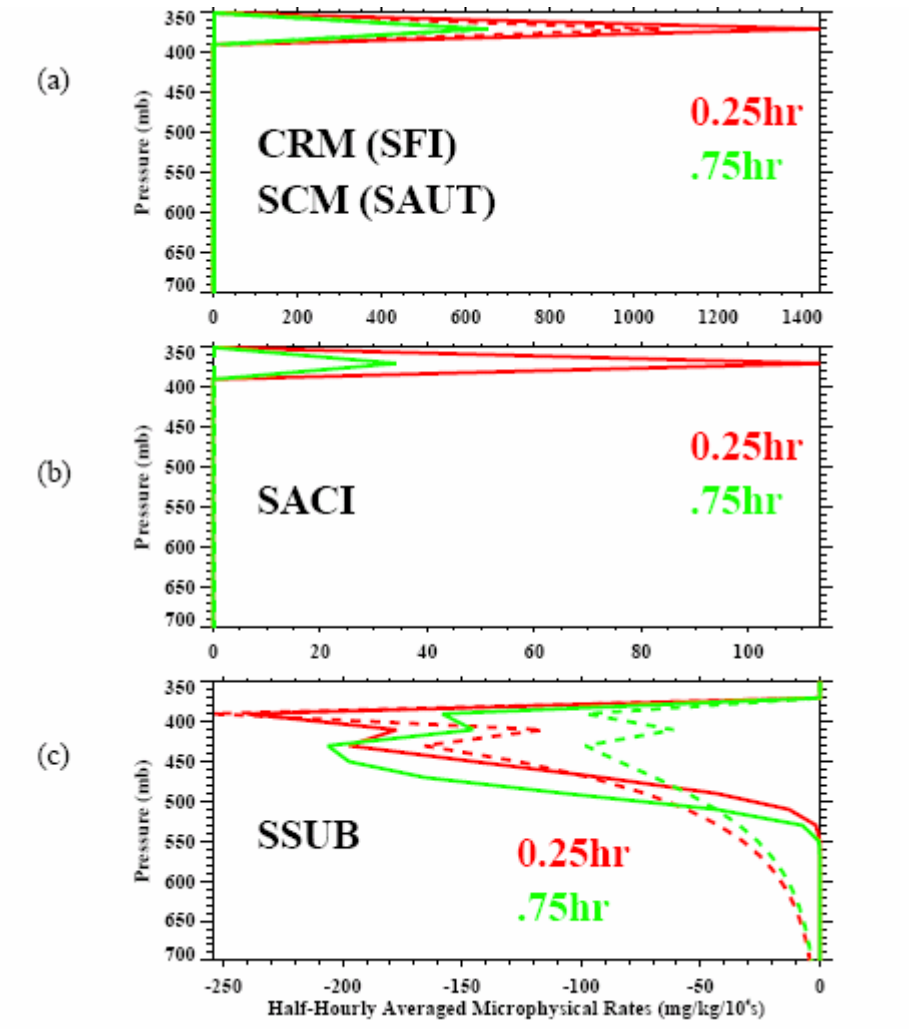


**Figure 4**. Profiles of the time-averaged rates (from 0 to 0.5 hr and 0.5 to 1.0 hr, respectively) of microphysical processes in Dscm (dashed lines) and Dcrm (solid lines) simulations. (a) Snow generation by Bergeron process in Dcrm and aggregation of ice in Dscm. (b) Snow generation by accretion of ice in Dscm. (c) Sublimation of snow in Dscm and Dcrm.

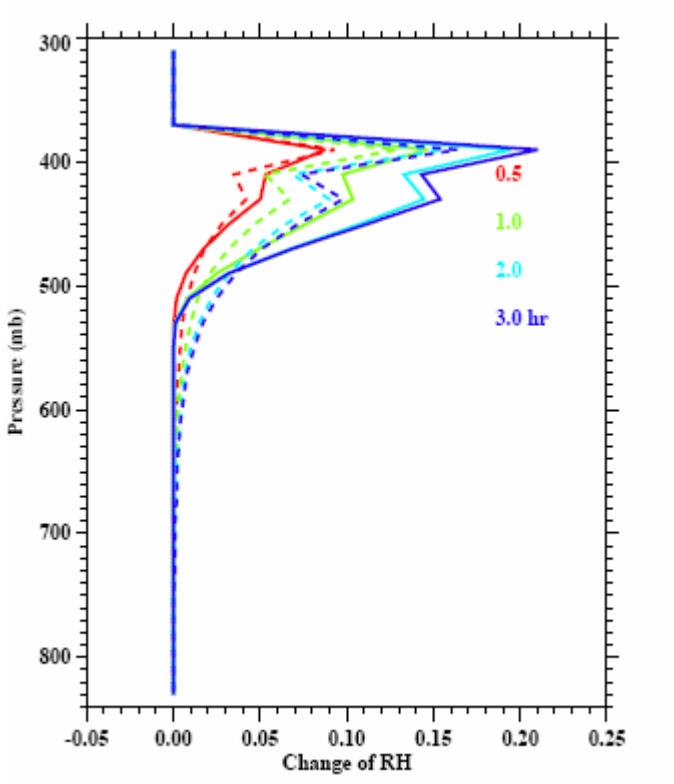


**Figure 5**. Profiles of the change of relative humidity from its initial value at 0.5, 1.0, 2.0, and 3.0 hr in Dcrm (solid lines) and Dscm (dashed lines) simulations.

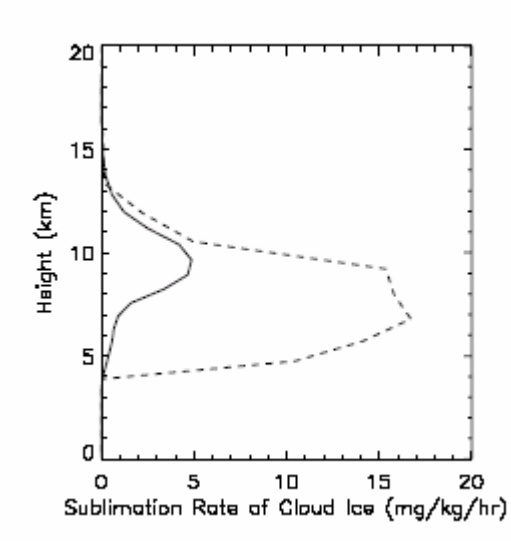


**Figure 6**. Profiles of sublimation rate of cloud ice in the CRM and SCM, averaged over the 29-day simulation period.

We cannot evaluate the SCM's cloud ice sublimation in the simulations just discussed in which cloud ice is detrained into a saturated layer. Instead, we analyzed the cloud ice sublimation rate in the SCM and CRM simulations performed using the large-scale forcing data at the ARM SGP site for the summer 1997 IOP. The profiles of the IOP averaged sublimation rate of cloud ice are compared (Figure 6). Cloud ice sublimation occurs from 4 to 15 km in the two simulations. Too much cloud ice is sublimated in the SCM at all layers where ice sublimation occurs, especially in the layer between 4 and 10 km. Luo et al. (2004, Figs 1 and 2) suggest that the overestimation of cloud ice sublimation in the SCM could contribute to a too moist atmosphere.

The time-height distributions of cloud ice sublimation are very different in the two models (Figure 7). Results during 5 days starting at July 7 23:30 UTC are provided for llustration, but similar features also are found during other subperiods of the IOP. The SCM's cloud ice sublimation has a similar distribution (Figure 7a) to that of its detrainment (Figure 2a). A great amount of cloud ice is sublimated when detrainment occurs. The sublimation occurs at a single layer at a time and too spontaneously. The CRM's sublimation appears to occur more smoothly in both height and time than the SCM. Sublimation occurs in the CRM during the 21th day of the IOP (between days 20 and 21 in Figure 7b) with maximal values at 8 to 11 km. From the second half of the 22th day to the end of the 23th day, relatively weak sublimation is simulated in the CRM.

The SCM's cloud ice amount and its changes by detrainment and microphysical processes for the 21th day at 9.2 km are shown as an example to demonstrate the impact on cloud ice by these physical processes (Figure 8). Approximately half of the detrained ice sublimates immediately after being detrained, and the other half decreases through conversion to precipitation (snow). The accretion of cloud ice by snow, another process included in the SCM, has a much smaller effect (not shown in Figure 8). This further demonstrates that sublimation along with cumulus detrainment are dominant processes determining cloud ice change in the SCM.

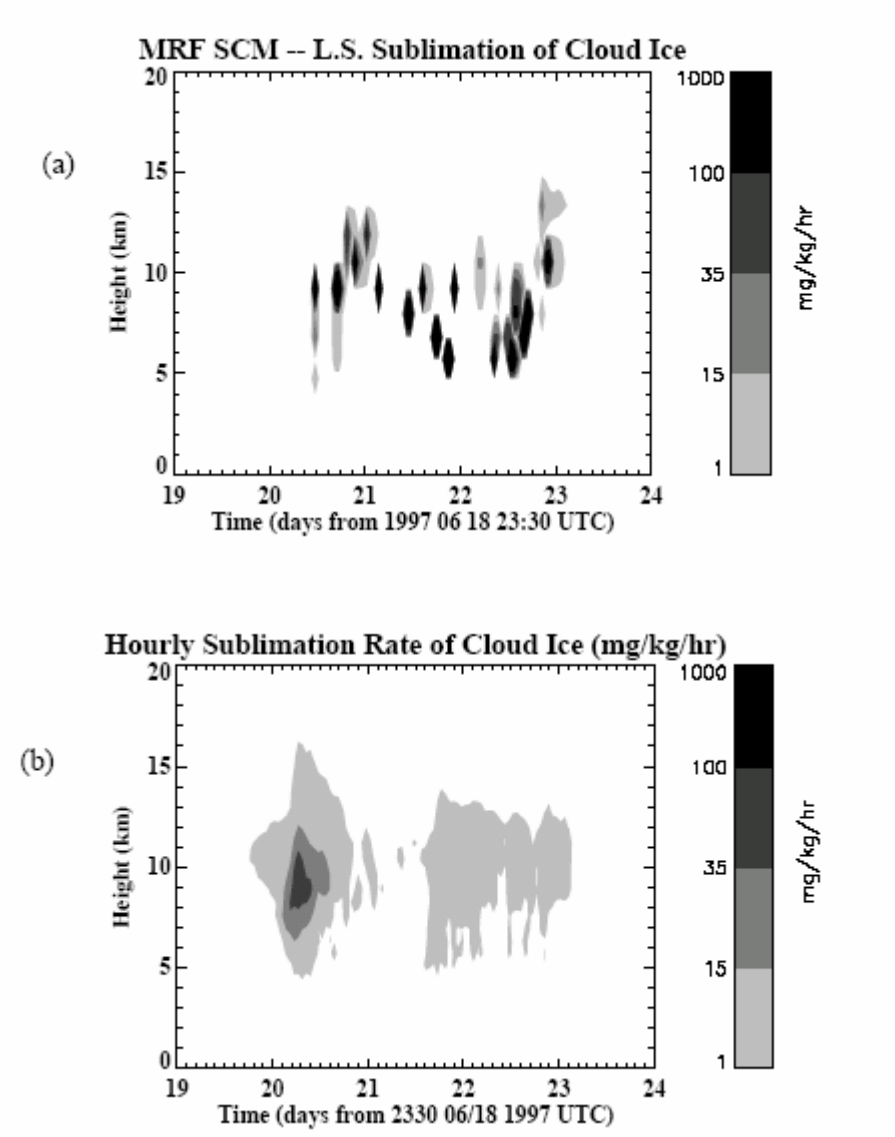


**Figure 7**. The time-height distributions of the hourly cloud ice sublimation rate in the SCM and CRM during a 5day subperiod of the IOP, starting at 23:30 UTC July 07 1997. (a) SCM. (b) CRM.

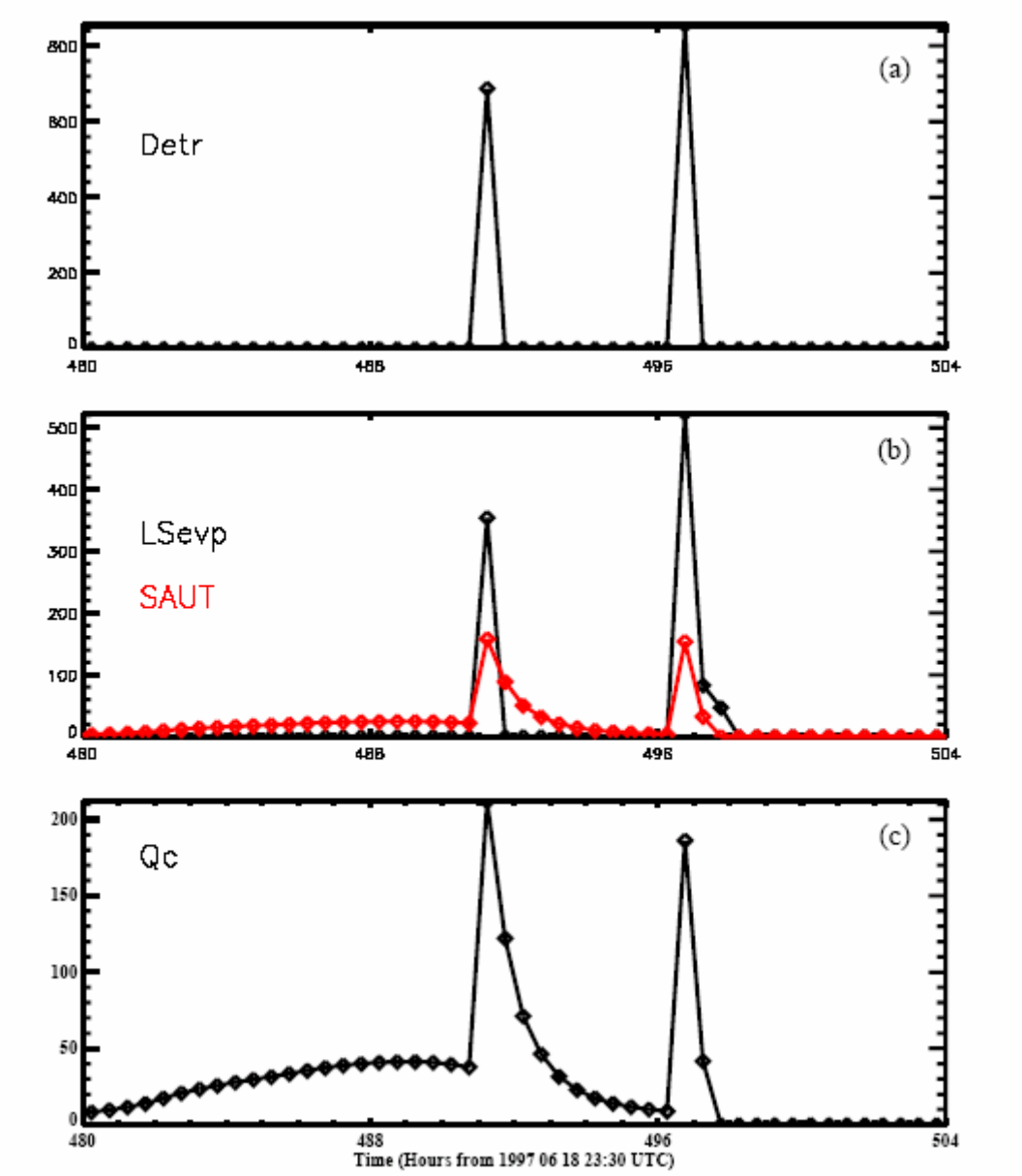


**Figure 8**. The SCM's cloud ice amount (mg kg$^{-1}$) and its change (over 0.5 hour) by detrainment and microphysical processes for the 21th day at 9.2 km. (a) Cloud ice change by detrainment. (b) Cloud ice change by large-scale sublimation and conversion to snow. (c) Cloud ice mixing ratio.

## Conclusions and Discussions

In Part I (Luo et al. 2004) the SCM simulated cirrus cloud properties were found to be very different from the cloud radar observations. Here, in Part II, we explore the possible reasons for these findings by comparing results from the SCM simulation to those from the CRM. We show that the reasons are closely related to the parameterizations of cumulus detrainment and cloud microphysical processes in

the SCM. With a correct time-averaged detrainment rate of cloud ice, but infrequent events combined with the assumption of no horizontal inhomogeneity of cloud ice, the SCM will not in general produce the correct cloud-scale statistics of cloud ice. Including multiple cloud types (detrainment levels) as the original Arakawa-Schubert scheme does is expected to help. Another possible improving method is to use a higher horizontal resolution and/or a smaller time step so that more of the possible detrainment levels will be sampled. The SCM diagnoses snow flux assuming that the net generation by microphysics is balanced by snow fall-out in one time step. When snow is included as cloud, this results in snow extending too low, and hence physically too thick cirrus layers with too low base-heights. Using a prognostic equation for snow may solve this problem. Cloud ice sublimates immediately after detrainment and at too large a rate in the SCM.

Using a prognostic equation for cloud fraction (e.g. Tiedtke 1993) may solve this problem. The detrained ice then simply increases the cloud fraction according to the volume of detrained air, where cloud ice evaporates at cloud boundaries by turbulent mixing of cloud air and unsaturated environmental air.

Results from our idealized 1-D simulations also show that for an overcast situation, while the rate of decrease of cloud ice by the CRM and SCM's microphysical processes are comparable, the dominant mechanism responsible for each is different. In the SCM it is transformation of cloud ice to snow via the aggregation of ice crystals in the SCM, while in the CRM it is via the growth of Bergeron-process embryos.

## Acknowledgements

This research was supported by the Environmental Sciences Division of the U.S. Department of Energy (DOE) as part of the Atmospheric Radiation Measurement program, under Grant DE-FG03-94ER61769. The authors thank Patrick Minnis' group at the NASA Langley Research Center for providing their cloud products.

## References

Ackerman, Thomas, and Gerry Stokes. 2003: The Atmospheric Radiation Measurement Program. *Physics Today*, **56**, 38 - 45.

Arakawa, A. and W. H. Schubert, 1974: Interaction of a cumulus ensemble with the large-scale environment, Part I. *J. Atmos. Sci.*, **31**, 674-704.

Cess, R. D., and coauthors, 1996: Cloud feedback in atmospheric general circulation models: An update. *J. Geophys. Res.,* **101***,* 12,791-12,794.

Del Genio, A. D., and M.-S. Yao, 1990: Predicting cloud water variations in the GISS GCM. Preprints, *Cof. on Cloud Physics*, San Francisco, CA, Amer. Meteor. Soc., 497-504.

Fowler, L. D., D. A. Randall, and S. A. Rutledge, 1996: Liquid and ice cloud microphysics in the CSU General Circulation Model. Part I: Model description and simulated microphysical processes. *J. Climate.*, **9**, 489-529.

Heymsfield, A., and J. Iaquinta, 2000: Cirrus crystal terminal velocities. *J. Atmos. Sci.*, **57**, 916938.

Krueger, S. K., 1988: Numerical simulation of tropical cumulus clouds and their interaction with the subcloud layer. *J. Atmos. Sci.*, **45**, 2221-2250.

--, and Y. Luo, 2004: Cloud properties simulated by a Single-Column Model. Part III: Cloud type radiative forcing and comparison with satellite observations and results from a CRM. To be submitted.

Lin, Y. L., R. D. Farley, and H. D. Orville, 1983: Bulk parameterization of the snow field in a cloud model. *J. Climate Appl. Meteor.*, **22**, 1065-1092.

Lord, S. J., H. E. Willoughby and J. M. Piotrowicz, 1984: Role of a parameterized ice-phase microphysics in an axisymmetric tropical cyclone model. *J. Atmos. Sci.*, **41**, 2836-2848.

Luo, Y.-L., and S. K. Krueger, 2004: Cloud types simulated by the NCEP GFS model. *Fourteenth Atmospheric Radiation Measurement (ARM) Science Team Meeting*, Albuquerque, New Mexico.

--, --, G. G. Mace, and K.-M. Xu, 2003: Cirrus cloud statistics from a cloud-resolving model simulation compared to cloud radar observations. *J. Atmos. Sci.,* **60**, 510-525.

--, --, and S. Moorthi, 2004: Cloud properties simulated by a single-column model. Part I: Comparison to cloud radar observations of cirrus clouds. Conditionally accepted by *J. Atmos. Sci.*.

Mace, G. G., E. E. Clothiaux, and T. P. Ackerman, 2001: The composite characteristics of cirrus clouds; bulk properties revealed by one year of continuous cloud radar data. *J. Climate,* **14**, 2185-2203.

Ose, T., 1993: An examination of the effects of explicit cloud water in the UCLA GCM. *J. Meteor. Soc. Japan*, **71**, 93-109.

Pan, H.-L., and W.-S. Wu, 1995: Implementing a mass flux convection parameterization package for the NMC medium-range forecast model. National Meteorological Center, Office Note 409, 40 pp. [Available from NCEP/EMC, 5200 Auth Road, Camp Springs MD 20746]

Randall, D., K.-M. Xu, R. J. C. Somerville, and S. Iacobellis, 1996: Single-column models and cloud ensemble models as links between observations and climate models. *J. of Climate.*, **9**, 1683-1697.

Randall, D., and coauthors, 2003: Confronting models with data. *Bull. Amer. Meteor. Soc.*, **84**, 455-469.

Stokes, G. M. and S. E. Schwartz, 1994: The Atmospheric Radiation Measurement (ARM) Program: Programmatic background and design of the Cloud and Radiation Testbed. *Bull. Amer. Meteor. Soc.*, **75**, 1201-1221.

Tiedtke, M., 1993: Representation of clouds in large-scale models. *Mon. Wea. Rev.*, **121**, 30403061.

Xu, K.-M., 1995: Partitioning mass, heat, and moisture budgets of explicitly simulated cumulus ensembles into convective and stratiform components. *J. Atmos. Sci.*, **52**, 551-573.

Zhang, M. H., and J. L. Lin, 1997: Constrained variational analysis of sounding data based on column-integrated budgets of mass, heat, moisture, and momentum: approach and application to ARM measurements. *J. Atmos. Sci.*, **54**, 1503-1524.

--, --, R. T. Cederwall, J. J. Yio, and S. C. Xie, 2001: Objective analysis of ARM IOP data: method and sensitivity. *Mon. Wea. Rev.*, **129**, 295-311.

Zhao, Q., and F. H. Carr, 1997: A prognostic cloud scheme for operational NWP models. *Mon. Wea. Rev.*, **125**, 1931-1953.